Article

Highly Hydrophilic TiO$_2$ Nanotubes Network by Alkaline Hydrothermal Method for Photocatalysis Degradation of Methyl Orange

Jin Yang [1], Jun Du [1,2,3,*], Xiuyun Li [1], Yilin Liu [1], Chang Jiang [1], Wenqian Qi [1], Kai Zhang [1], Cheng Gong [1], Rui Li [1], Mei Luo [1] and Hailong Peng [1,3,*]

[1] Key Lab of Poyang Lake Environment and Resource Utilization (Ministry of Education), Nanchang University, Nanchang 330031, China; yangjin199501@sina.com (J.Y.); show7898@foxmail.com (X.L.); 15079171252m0@sina.cn (Y.L.); 16607001729y@sina.com (C.J.); qiwenqian9873@sina.com (W.Q.); zhangkai7755@sina.com (K.Z.); stokescheng@sina.com (C.G.); lr3132@sina.com (R.L.); luomei@ncu.edu.cn (M.L.)

[2] Jiangxi Province Key Laboratory of Edible and Medicinal Plant Resources, Nanchang University, Nanchang 330031, China

[3] Department of Chemical Engineering, School of Environmental and Chemical Engineering, Nanchang University, Nanchang 330031, China

* Correspondence: dujun@ncu.edu.cn (J.D.); penghailong@ncu.edu.cn (H.P.); Tel.: +86-791-83969985 (J.D. & H.P.)

check for updates

Abstract: High-density and highly cross-coated anatase TiO$_2$ nanotubes networks have been successfully prepared on the surface of Ti foil by alkaline hydrothermal using NaOH and Ti foil as the precursors. The nanotubes networks were analyzed using X-ray diffraction (XRD), energy dispersive X-ray spectrometer (EDX), transmission electron microscope (TEM), scanning electron microscopy (SEM), optical contact angle tester, and ultraviolet (UV) fluorescence spectrophotometer, respectively. The results showed that the nanotubes network with diameters of 30–50 nm were obtained on the Ti foil surface. The morphology of the nanotubes network possessed the three-dimensional network structure, The TiO$_2$ nanotubes network grew along the (101) direction of the tetragonal anatase crystal. The morphology and crystal phase of the TiO$_2$ nanotubes network were better at the conditions of NaOH concentration 7–10 mol/L and temperature 160–170 °C. The best contact angle of TiO$_2$ nanotubes network after UV-light irradition was only 5.1 ± 2.9°. Under the irradiation of mercury lamp, the nanotubes network exhibited excellent photocatalytic performance and the degradation ratio of methyl orange solution reached to 80.00 ± 2.33%. Thus, the anatase TiO$_2$ nanotubes network has great potential in applications for pollution photocatalytic degradation.

Keywords: titanium dioxide; nanotubes network; photocatalysis; alkaline hydrothermal method; hydrophilicity

1. Introduction

In recent years, a large number of pollutants have been found in various types of water bodies [1], from surface water to groundwater resources [2,3]. Therefore, how to deal with water pollution has become an urgent problem to solve. Photocatalysis is a new technology developing rapidly in recent years to make use of solar energy for environmental purification and energy conversion [4]. As a photocatalyst, TiO$_2$ can completely and rapidly degrade various toxic compounds and oxidize acids, dyes, organic phosphorus pesticides, fuel oil, and other organic N-containing compounds in water into CO$_2$, H$_2$O, and other non-toxic substances [5]. Therefore, TiO$_2$ has been widely used in the fields

of water treatment and air purification for its features of chemical stability, insolubility, light corrosion resistance, non-toxicity, and low cost [6–13].

Nowadays, different forms of nano-TiO_2 have attracted extensive attention due to their improved toxic compounds degradation and photocatalytic performance, such as nanoparticles [14], nanobelts [15], nanowires [16], nanorods [17], nanotubes [18] and nanoflowers [19]. Meanwhile, nanotubes not only have chemical stability but also superior photocatalytic properties. Therefore, more and more researchers are doing research into nanotubes. Sreekantan et al. used commercial titania nanoparticles as starting material to carry out hydrothermal reaction in aqueous sodium hydroxide solution, and the prepared anatase TiO_2 nanotubes exhibited excellent photocatalytic performance [20]. Sun et al. successfully prepared TiO_2 nanotubes on carbon fibers substrate using TiO_2 nanowires as reaction materials [21]. Up to now, various methods have been used to prepare nanotubes, such as templating synthesis method [22], sol-gel method [23], anodization method [24], and hydrothermal method [25]. Among them, the hydrothermal method has the advantages of low reaction temperature and easy to obtain. Additionally, the nanotubes prepared by the hydrothermal method have high purity and a good crystal phase. Therefore, hydrothermal synthesis has a broad developing prospect in preparation of nano-materials [26].

At present, the main preparation substrate of TiO_2 nano-materials were the glass, absorbent (activated carbon, Silica gel, etc.) and metal. However, glass when used as a substrate has its limitations of poor combination degree with TiO_2, leading to TiO_2 being easily detached from the substrate. The absorbents were used as a substrate, which not have conductivity. In order to overcome the disadvantages of these substrate, Ti foil has been used as the TiO_2 nano-materials precursor and the substrate. Ti foil has excellent conductivity and is not easy to break. TiO_2 nano-materials were directly grown from Ti foil, not only made it avoid the complicated preparation of precursor reactants, but also can fix tightly on the Ti foil. Moreover, the TiO_2 nano-materials grown from Ti foil have many advantages of high yield and high density. Thus, Ti foil was the excellent substrate for the practical application of TiO_2 nanomaterials.

In this study, high-density anatase TiO_2 nanotubes network were successfully prepared using alkaline hydrothermal method on the surface of Ti foil. The novelty of this work has been demonstrated as follows: (1) the TiO_2 nanotubes network are grown directly on the Ti foil surface using alkaline hydrothermal method with excellent photocatalytic and hydrophilic properties; (2) the TiO_2 nanotubes network and Ti foil are tightly connected, which facilitates recycling in the application to prevent secondary pollution; (3) the effect of NaOH concentration and hydrothermal temperature on TiO_2 nanotubes network morphology and properties has been demonstrated.

2. Experiment

2.1. Materials

Ti foil was purchased from Tenghui Titanium Factory (Jinhua, China). Sodium hydroxide (NaOH) and Anhydrous ethanol (C_2H_5OH) were obtained from Tianjin Da Mao chemical reagent factory (Tianjin, China). Methyl orange (MO) was purchased from Shanghai Zhanyun Chemical Co., Ltd. (Shanghai, China). Acetone (C_3H_6O) was purchased from Shanghai Yanchen Chemical Industrial Co., Ltd. (Shanghai, China). The deionized water was obtained from a Mili-Q Ultrapure water system (Millipore, Bedford, MA, USA).

2.2. Preparation of TiO_2 Nanotubes Network

The Ti foil was successively placed in acetone solution, anhydrous ethanol and deionized water for ultrasonically cleaned to remove the oxide and residual oil on the surface of the Ti foil. NaOH (60 mL, 1–10 mol/L) and Ti foil (50 × 30 × 3 mm) were added to the polytetrafluoroethylene liner, respectively. It was noted that the Ti foil must be lie vertically on the edge of the polytetrafluoroethylene liner. It can increase the contact area between Ti foil and NaOH. Next, the polytetrafluoroethylene liner was placed

in a high pressure reactor for 4 h in the reaction chamber at a temperature of 130–170 °C. When the high pressure reactor reached room temperature, the Ti foil was taked out from the polytetrafluoroethylene liner, and then rapidly added into HCl solution (0.1 mol/L) for pickling for 12 h. Finally, the Ti foil was dried in a vacuum drying oven at 50 °C and was inserted into the muffle furnace (500 °C) to anneal for 2 h. After that, the TiO$_2$ nanotubes network was formed. The preparation process was as follows (Scheme 1).
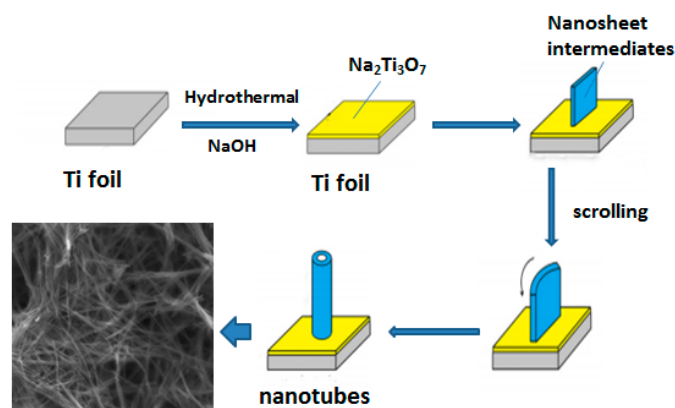
Scheme 1. Preparation processes of TiO$_2$ nanotubes network.

2.3. Characterization

X-ray diffractometry (XRD, Bede, Durham, UK) was performed to characterize the phase structure of the samples, X-ray diffractometer with CuKα (λ = 0.15406 nm) radiation operated at 40 kV and 35 mA, Diffractograms were collected in between 10° to 8°. A field emission scanning electron microscope (FESEM, FEI Quanta200F, FEI, Hillsboro, OR, USA) was used to identify the morphology of the as-deposited material, experimental testing requires high-vacuum conditions, the sample was cut into a square with a side length of 10 mm, the sample is closely attached to the sample stage with conductive tape, and the sample is amplified by different multiples for detection. High-resolution transmission electron microscope (HRTEM) images were obtained on a JEOL-2010 HRTEM (JEOL, Tokyo, Japan) using an acceleration voltage of 200 kV, TEM grids were prepared by dispersing samples in Anhydrous ethanol (5 min ultrasonication) and then dropping onto a carbon Cu grid. The sizes of nanotubes network were determined by the scale plate in the TEM and SEM images. The photocatalytic reaction was carried out in a photochemistry reaction instrument (BL-GHX-V, BILON, Shanghai, China), photochemistry reaction instrument (480 mm × 420 mm × 900 mm) is a sealed rectangular parallelepiped structure, The sample was added into a quartz reaction tube with 35 mL MO (20 mg/L) for photocatalytic degradation, and a 500 W high pressure mercury lamp was used as the light. The hydrophilic properties were observed on the optical contact angle measuring instrument (Zheke, DSA 100, Zheqi Technology, Beijing, China), Dropping a drop of deionized water on the sample surface was employed by the hanging drop method to determine the contact angle of the droplet with the sample.

2.4. Photocatalytic Reactions of TiO$_2$ Nanotubes Network

The TiO$_2$ nanotubes network sample was cut into a square with a side length of 10 mm, which was added into a quartz reaction tube with 35 mL MO (20 mg/L) for photocatalytic degradation. MO (20 mg/L) standard solution with the concentration of 1–40 mg/L had a good linear relationship with absorbance. The 500 W high-pressure mercury lamp with a main wavelength of 365 nm was used as the light source. The effective area of TiO$_2$ nanotube network for photocatalytic reaction was 1 cm^2. The light intensity was measured as 160 mW/cm^2 in the reaction system. This was taken out the MO solution every 15 min and tested for absorbance. The photocatalytic performance is determined by the degradation rate (η), which is calculated as follows [27]:

$$\eta = \frac{C_0 - C}{C_0} \times 100\% = \frac{A_0 - A}{A_0} \times 100\% \quad (1)$$

where C_0 and C are the initial concentration and the concentration of MO at different time, A_0 and A are the initial absorbance and absorbance of MO at 466 nm under ultraviolet (UV) light irradiation at different time.

3. Results and Discussion

3.1. Formation and Photocatalytic Mechanism of TiO$_2$ Nanotubes Network

The formation mechanism of TiO$_2$ nanotube network can be explained by the following three stages. Firstly, Ti foil can react with NaOH to form titanate hydrogel, the fracture of titanate hydrogel is recombined into layered Na$_2$Ti$_3$O$_7$. As the reaction proceeded, the layered Na$_2$Ti$_3$O$_7$ continuous grown on the Ti foil surface, a multilayer nanotube film covering the Ti foil surface was formed. Then, Na$^+$ was replaced by H$^+$ in the process of pickling with HCl, and the reaction produced H$_2$Ti$_3$O$_7$. Finally, the H$_2$Ti$_3$O$_7$ was annealed at high temperature, and the anatase TiO$_2$ nanotubes network were prepared after dehydration of titanite and lattice rearrangement. The reaction scheme of the TiO$_2$ nanotubes network formations is given below:

$$3Ti + 2NaOH + 5H_2O \rightarrow Na_2Ti_3O_7 + 6H_2 \text{ (g)} \quad (2)$$

$$Na_2Ti_3O_7 + 2HCl \rightarrow H_2Ti_3O_7 + 2NaCl \quad (3)$$

$$H_2Ti_3O_7 \rightarrow 3TiO_2 + H_2O \quad (4)$$
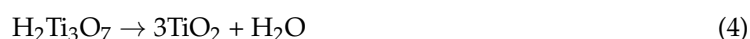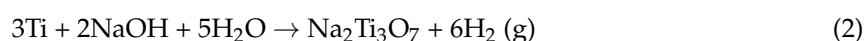
When ultraviolet light irradiated on the surface of TiO$_2$, the electron was excited from the valance band to the conduction band. Therefore, highly active photogenerated electrons (e$^-$) and holes (h$^+$) were produced on the conduction and valence bands. Dissolved oxygen (O$_2$) captures the electron to form atomic oxygen ($\cdot$O^{2-}), and the holes oxidize OH$^-$ and H$_2$O adsorbed on the surface of the catalyst to form hydroxyl radicals ($\cdot$OH), which can degrade most organic pollutants into carbon dioxide and water, and degrade inorganic pollutants into harmless substances. The photocatalytic mechanisms of TiO$_2$ towards the degradation of MO is that the h+ react with H$_2$O to form $\cdot$OH, $\cdot$OH oxidize and degrade MO, and the azo bond and benzene ring of MO are broken to produce H$_2$O, CO$_2$, SO$_4{}^{2-}$ and NO$_3{}^-$ to achieve the degradation effect. The photocatalytic mechanism of TiO$_2$ is given below:

$$TiO_2 + hv \rightarrow TiO_2 \text{ (h}^+ + \text{e}^-) \quad (5)$$

$$h^+ + OH^- \rightarrow \cdot OH \quad (6)$$

$$h^+ + H_2O \rightarrow \cdot OH + H^+ \quad (7)$$

$$e^- + O_2 \rightarrow \cdot O^{2-} \quad (8)$$
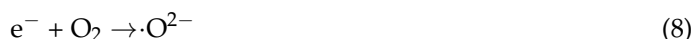
3.2. Characterizations of TiO$_2$ Nanotubes Network

Figure 1 shows the XRD patterns of different reaction stages of hydrothermal reaction. According to the XRD standard card of Ti (PDF NO. 44-1294), the diffraction peaks located at 38.42°, 40.17°, 53.0°, 62.94° and 70.66° was correspond to the (002), (101), (102), (110), and (103) planes of Ti (Figure 1a). The diffraction peaks of samples located at 24.32°, 28.35° and 47.78° without washing with HCl, which correspond to the (102), (111) and (020) planes of Na$_2$Ti$_3$O$_7$ (Figure 1b), according to the XRD standard card of Na$_2$Ti$_3$O$_7$ (PDF NO.72-0148). After the hydrothermal reaction, the diffraction peaks located at 24.37° and 48.52°, which correspond to the (102) and (020) planes of H$_2$Ti$_3$O$_7$ (Figure 1c). After the sample was washed with HCl and high-temperature annealing, the diffraction peak of titanate was disappeared and the diffraction angles (2θ) of 25.3°, 48.04°, 53.88° and 55.06° correspond to the (101),

(200), (105) and (211) planes for anatase TiO_2 (Figure 1d). These results showed that an anatase TiO_2 crystal phase has formed.
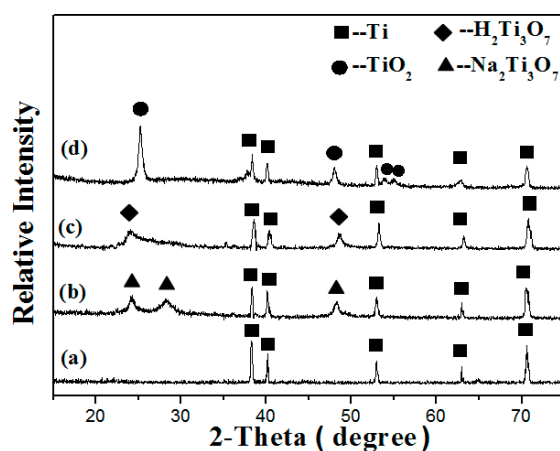

Figure 1. X-ray diffraction (XRD) patterns of samples. (a) Ti foil; (b) intermediate on the Ti foil; (c) intermediate product after pickling is on the Ti foil; (d) TiO_2 nanotubes network.

Scanning electron microscope (SEM) micrographs of the samples prepared at different reaction stages of hydrothermal reaction are shown in Figure 2. Figure 2a showed that the surface of the Ti is not flat with some steps and cracks, but there is no a linear structure. From Figure 2b, it can be seen that the Ti foil surface was dense and irregular $Na_2Ti_3O_7$ with the size of about 2 µm. Figure 2c showed that $H_2Ti_3O_7$ was obtained after washing with HCl, the Ti foil surface was covered with dense and uniform nanotubes, and the growth of the nanotubes has no fixed direction. The nanotubes were randomly grown on the surface of the Ti foil to form a network structure, and the diameter of the nanotubes were approximately 30 nm. Figure 2d showed the micrograph of the TiO_2 after the sample was high-temperature annealed. Compared with the network structure of $H_2Ti_3O_7$ nanotubes, the network structure of TiO_2 nanotubes were more slender and looser, and have better cross-over in the longitudinal direction. The network structure of TiO_2 nanotubes can help internal TiO_2 nanoparticles to more use during the reaction processes.
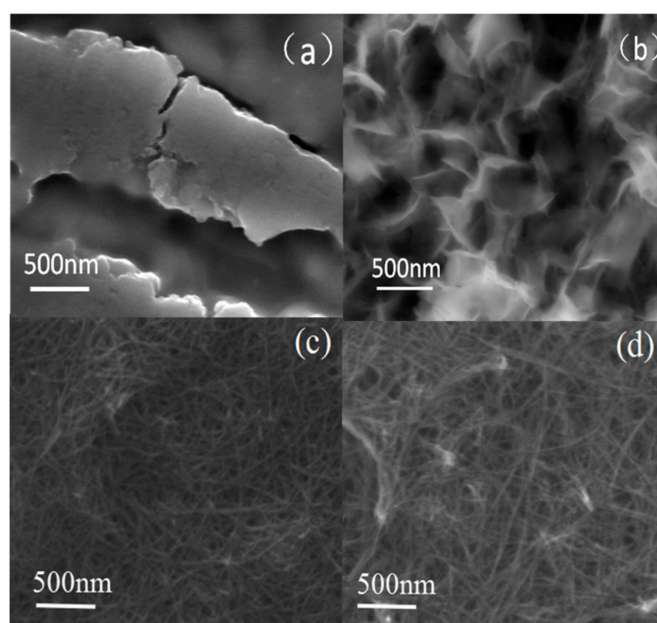

Figure 2. Scanning electron microscope (SEM) images of samples. (**a**) Ti foil; (**b**) intermediate on the Ti foil; (**c**) intermediate product after pickling is on the Ti foil; (**d**) TiO_2 nanotubes network.

Figure 3 showed the XRD patterns of the TiO_2 nanotubes network prepared on Ti foil surface with different NaOH concentrations at 160 °C for 4 h. Obviously, four strong diffraction peaks at 2θ values of 38.42°, 40.17°, 53.0° and 62.94° were found in Figure 3. According to the XRD standard card of pure Ti (PDF NO. 44-1294), the diffraction angles (2θ) of 38.42°, 40.17°, 53.0° and 62.94° correspond to the (002), (101), (102), and (110) planes for Ti, respectively. This indicated that the Ti substrate always exists. Additionally, new diffraction peaks appeared at 2θ of 25.3° and 48.04° and its intensity increased with the concentration of NaOH solution increasing. Compared with the XRD standard card of TiO_2 (PDF NO. 78-2486), it is obvious that the diffraction angles (2θ) 25.3° and 48.04° were separately characterized as the (101) and (200) planes for anatase TiO_2, respectively. This result showed that the anatase TiO_2 crystal phase was formed. The Ti foil was not enough to react with the low concentration of NaOH to form titanate hydrogels until the concentration of NaOH solution was increased to 3 mol/L. When the NaOH concentration increases from 3 mol/L to 10 mol/L, the content of TiO_2 crystal continuously increased. These results indicated that a certain thickness of anatase TiO_2 crystal was formed in the Ti foil surface.
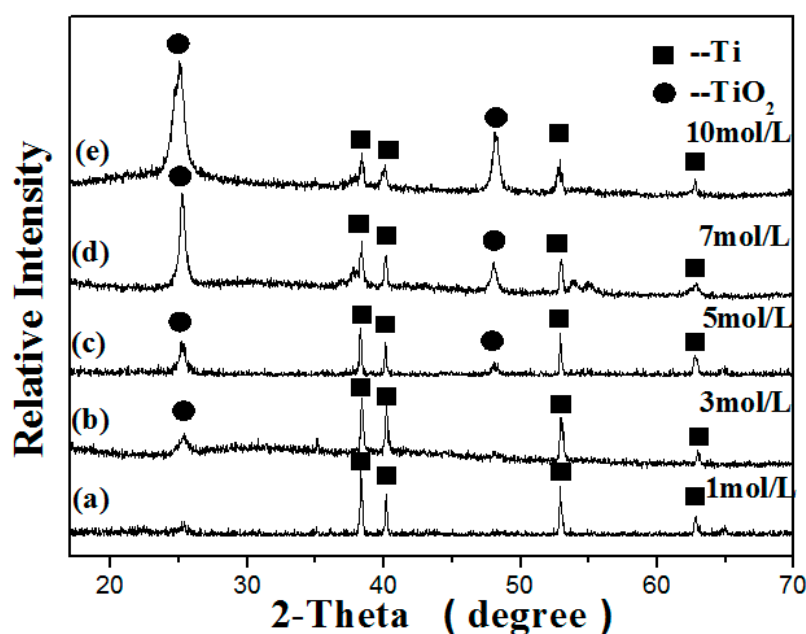

Figure 3. XRD patterns of samples prepared at the different concentration of NaOH. (a) 1 mol/L; (b) 3 mol/L; (c) 5 mol/L; (d) 7 mol/L; (e) 10 mol/L.

SEM micrographs of TiO_2 nanotubes network were shown in Figure 4 with different NaOH concentrations. As shown in Figure 4, the flake or layered structure was gradually transformed into more elongated nanotubes, and the nanotubes were interwoven together to form a network structure. Low NaOH concentration is not sufficient to allow the Ti foil dissolved continuously. When the NaOH concentration increased to 5 mol/L, the layered film was cracked into a bundle structure interwoven together, and each bundle had a diameter of about 100 nm (Figure 4c). When the NaOH concentration continue to increase, the nanotubes with diameter of 50 nm can be observed (Figure 4d). At this time, the nanotubes were structurally intact and uniform size, and the nanotubes interwoven together to form micropores with the diameter of 100 nm. The density of the nanotubes became larger when the NaOH concentration increased to 10 mol/L, and the nanotubes became more slender with diameter of about 30 nm (Figure 4e). Obviously, more Ti react as the concentration of NaOH increases. Meanwhile, the density of TiO_2 nanotubes gradually increased with the NaOH concentration increasing, which was consistent with the result of XRD.
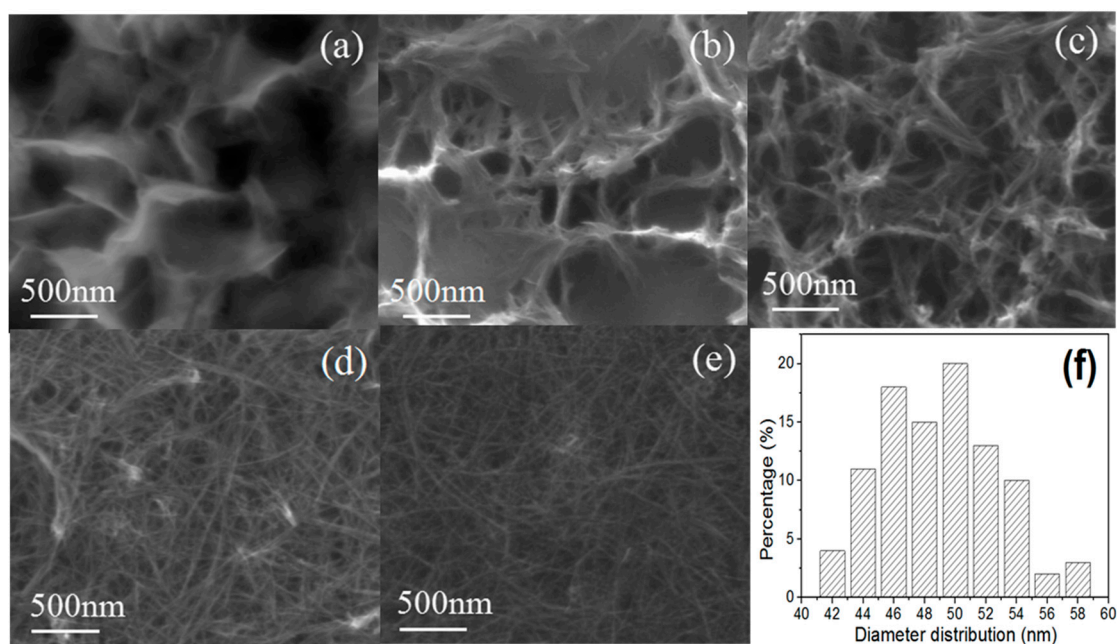
Figure 4. SEM micrographs of TiO$_2$ nanotubes prepared at the different concentration of NaOH. (**a**) 1 mol/L; (**b**) 3 mol/L; (**c**) 5 mol/L; (**d**) 7 mol/L; (**e**) 10 mol/L; (**f**) the size distribution of TiO$_2$ nanotubes prepared under conditions of 7 mol/L NaOH.

Figure 5 shows the XRD patterns of TiO$_2$ nanotubes network prepared on Ti foil surface with different hydrothermal temperature under conditions of 7 mol/L NaOH for 4 h. According to the XRD standard card of TiO$_2$ (PDF NO. 78-2486), the diffraction peaks located at 25.3° and 48.04° corresponded to the (101) and (200) planes for anatase TiO$_2$ (Figure 5). When the hydrothermal temperature increased from 130 °C to 170 °C, the diffraction peaks of anatase TiO$_2$ was increased and the diffraction peaks of Ti decreased, which indicated that the TiO$_2$ grows with consuming of Ti. When the temperature was 130 °C, the dissolved precursor concentration was low, and it was not good for the anatase TiO$_2$ nanotubes network to grow. The Ti dissolution in NaOH solution was accelerated with the increasing of hydrothermal temperature, which makes the reaction faster. Therefore, the temperature increasing can promote growth of the TiO$_2$ nanotubes network.
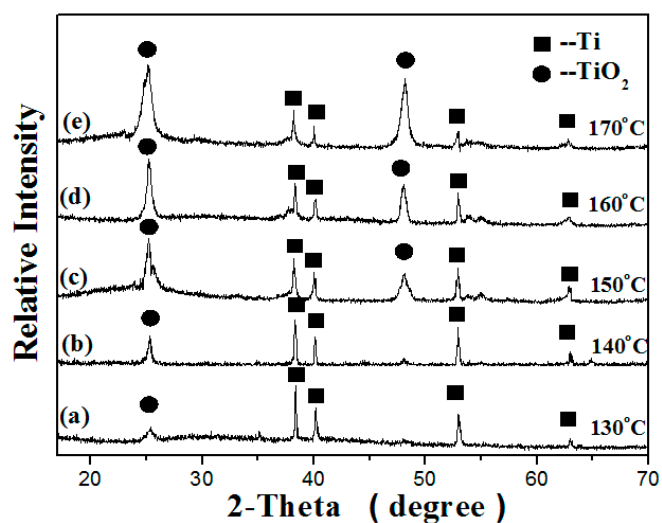

Figure 5. XRD patterns of samples prepared at different temperatures. (a) 130 °C; (b) 140 °C; (c) 150 °C; (d) 160 °C; (e) 170 °C.

The corresponding morphologies of the TiO_2 nanotube network prepared at different reaction temperature were shown in Figure 6. When the temperature was 130 °C, the nanotube interwoven together to form deep holes with diameter of about 2 μm. At such a temperature, the Ti foil surface could not be completely reacted. When the temperature continued to increase, the deep holes were getting smaller and smaller, and the deep holes were about 1 μm in diameter at 150 °C. It can be clearly seen that deep holes were slowly filled with TiO_2 nanotubes (Figure 6b,c). When the reaction temperature increases to 160 °C, the TiO_2 nanotubes formed, and the diameters of the nanotubes were approximately 50 nm. Meanwhile, the nanotubes intersected to form a highly dense network structure (Figure 6d). When the reaction temperature increases to 170 °C, the deep holes disappeared completely (Figure 6e) and the diameter of the nanotubes little changed, and the nanotubes network on the Ti foil surface was stodgier.
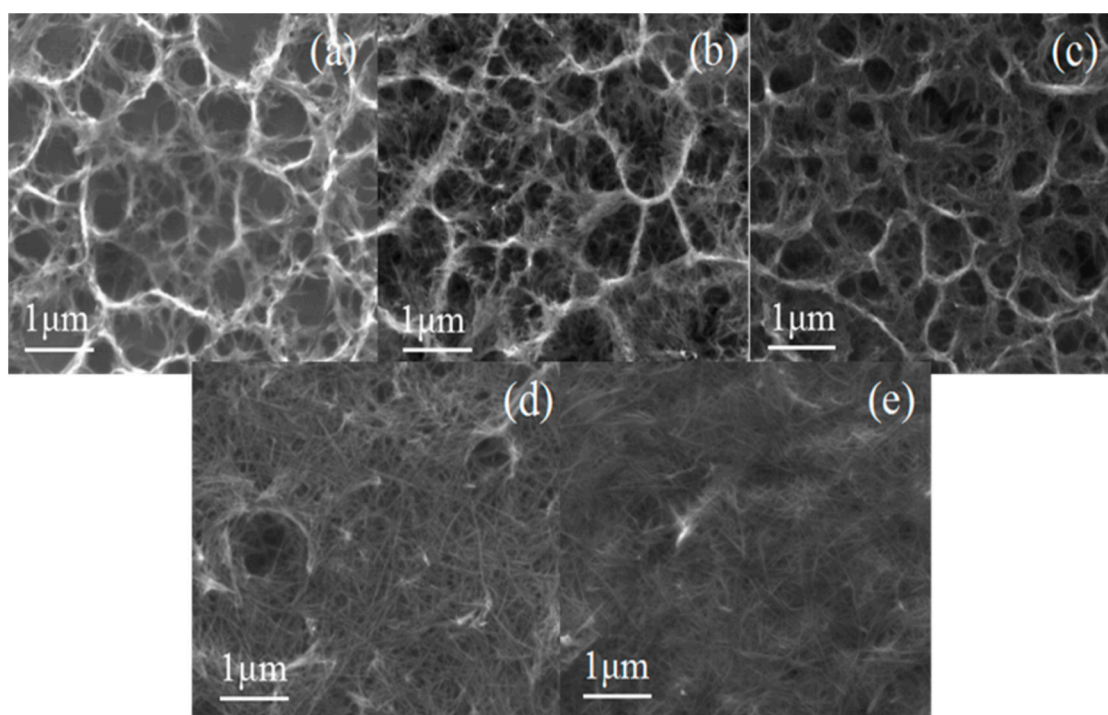

Figure 6. SEM images at different temperatures. (**a**) 130 °C; (**b**) 140 °C; (**c**) 150 °C; (**d**) 160 °C; (**e**) 170 °C.

The characterization of the TiO_2 nanotubes are shown in Figure 7. As shown in Figure 7a, it can be concluded that the nanotubes were composed of Ti and O elements. Cu element and C atom generated from copper grid and carbon film on the copper grid [21], respectively. Some approximately 2 μm long nanotubes with a diameter of 50 nm are shown in Figure 7b, which was in good agreement with the SEM micrographs. The four diffraction rings of d_1, d_2, d_3, and d_4 were consistent with the (101), (200), (105) and (211) crystallographic planes of TiO_2 (Figure 7c), respectively, which was consistent with the XRD standard card of TiO_2 (PDF NO. 78-2486). Regular lattice fringes can be seen clearly in the high-resolution transmission electron microscope (HRTEM) image and *d*-spacings of crystallographic planes were 0.354 nm, which is consistent with (101) crystallographic planes of TiO_2 (Figure 7d). According to the XRD pattern and the energy dispersive X-ray (EDX) spectrum, it can be clearly concluded that these nanotubes were anatase TiO_2 nanotubes.
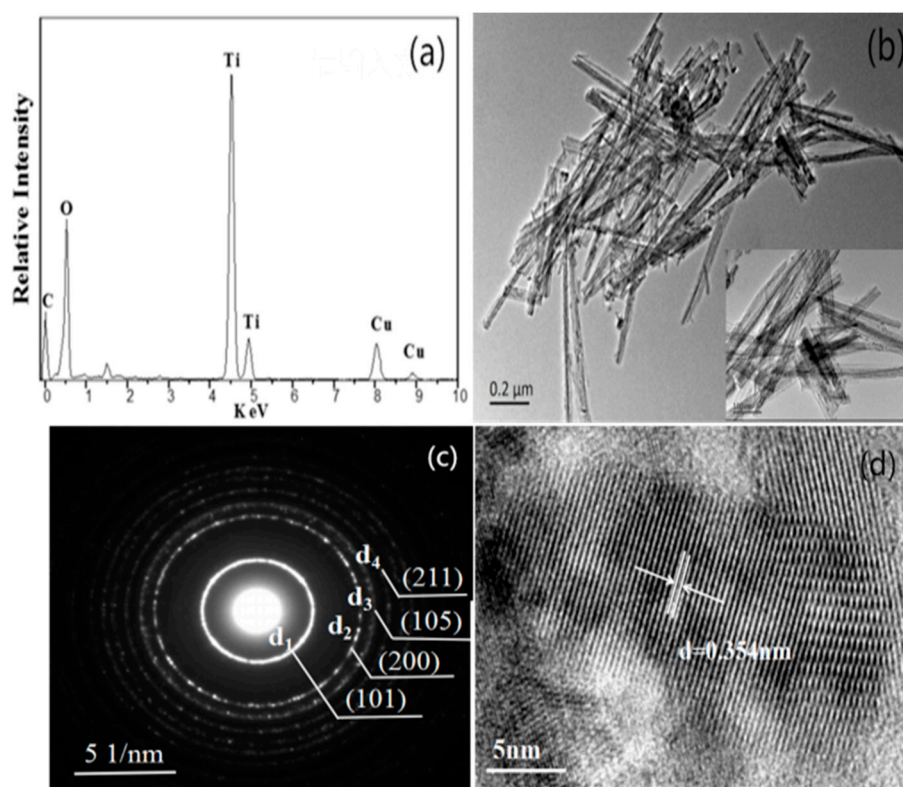
Figure 7. Characterization of TiO$_2$ nanotubes. (**a**) energy dispersive X-ray (EDX) spectra of TiO$_2$ nanotubes. (**b**) Transmission electron microscope (TEM) image of TiO$_2$ nanotubes. (**c**) Electron diffraction pattern of the TiO$_2$ nanotubes. (**d**) High-resolution transmission electron microscope (HRTEM) image of the TiO$_2$ nanotubes.

3.3. Hydrophilicity of TiO$_2$ Nanotubes Network

Ultraviolet (UV) light stimulates the TiO$_2$ surface to produce electron hole pair, which restores Ti^{4+} and oxidizes O^{2-}, leading to the generation of oxygen vacancy. The vacancy reacted with surface hydroxyl groups and absorbed H$_2$O and form hydroxyl radicals [28]. More and more H$_2$O was absorbed by hydroxyl radicals and then presented super-hydrophilic performance [29]. The hydrophilicity of TiO$_2$ nanotube network grown at different concentrations of NaOH solution and temperatures is shown in Figure 8. The optical contact angle of the sample was 88 $\pm$ 2.9° when the NaOH concentration was 1 mol/L (Figure 8a), and the optical contact angles were 8.9 $\pm$ 2.9° and 5.1 $\pm$ 2.9° when NaOH concentrations were 7 mol/L and 10 mol/L, respectively. When NaOH concentration increased from 1 mol/L to 7 mol/L, more TiO$_2$ crystal phase was produced. Therefore, the hydrophilicity of the TiO$_2$ sample increased continuously. The Ti foil surface was completely covered by TiO$_2$ crystal phase at NaOH concentration of 7 mol/L, and the physical adsorption and chemical adsorption of water molecules had reached saturation. Meanwhile, the optical contact angle of the sample was 8.9 $\pm$ 2.9° and 6.5 $\pm$ 2.9 °C when the reaction temperature was 160 °C and 170 °C, respectively. Therefore, the hydrophilicity of the sample was best when NaOH concentration and reaction temperature were 10 mol/L and 160 °C, respectively.
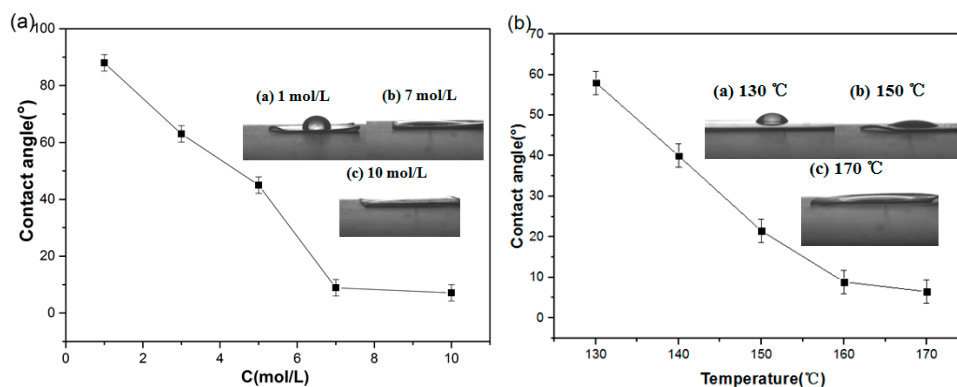
Figure 8. Hydrophilic property of TiO$_2$ nanotubes network prepared at (**a**) different concentration of NaOH; (**b**) different temperatures.

3.4. Photocatalytic Reaction of TiO$_2$ Nanotubes Network

Figure 9 shows the photodegradation behavior of MO solution in the presence of the TiO$_2$ nanotubes network grown at different NaOH concentrations and different reaction temperatures (Figure 9a,b). When the NaOH concentration solution was 1 mol/L, few TiO$_2$ crystal phase were prepared by hydrothermal reaction and the ratio of photocatalytic degradation was only $11.00 \pm 2.33\%$. The degradation ratio gradually increased with the NaOH concentration increasing. When the concentration of NaOH solution of hydrothermal reaction was 7 mol/L, the relative concentration of MO reaches the minimum with the degradation ratio of $80.00 \pm 2.33\%$. The photocatalytic degradation ratio of TiO$_2$ nanotubes was slightly lower than that of 7 mol/L when the NaOH concentration was 10 mol/L, which was due to the TiO$_2$ nanotube density causing the micropore size decrease and inhibiting the reactants from reaching the internal active sites. Therefore, the photocatalytic performance of the TiO$_2$ nanotube network was best when the concentration of NaOH solution was 7 mol/L.
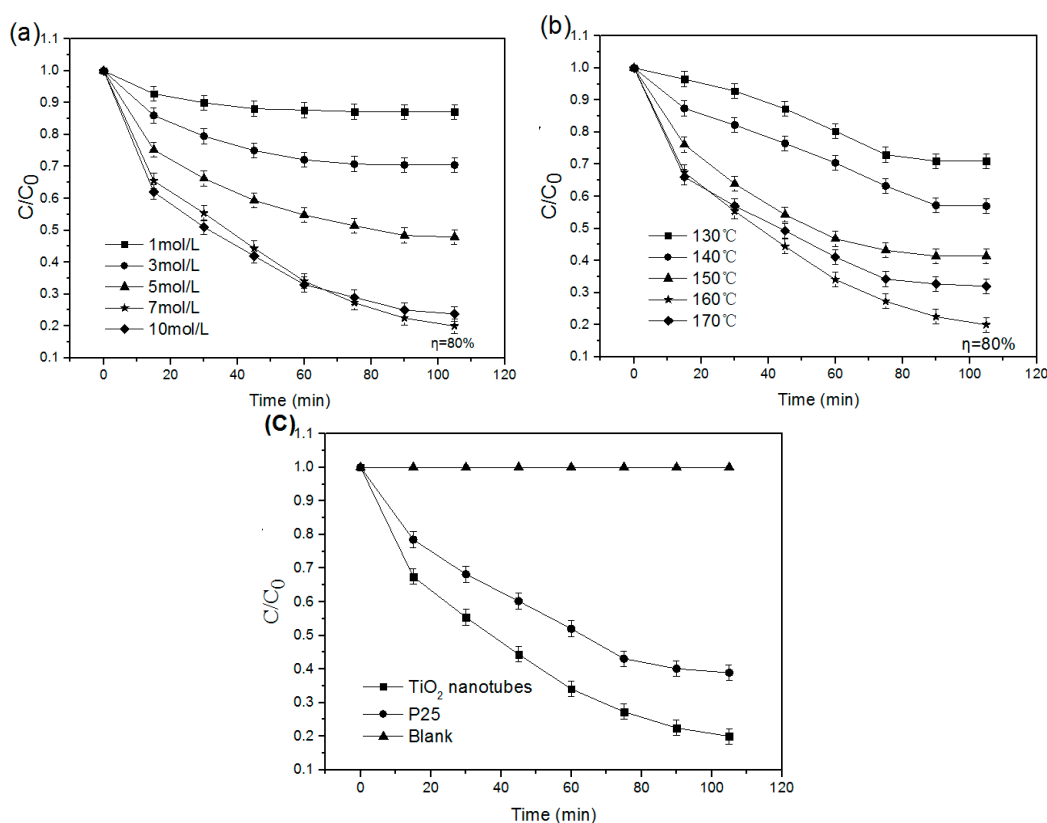

Figure 9. Variation of C/C$_0$ of MO (20 mg/L) solution with the photocatalytic time.

As shown in Figure 9b, the degradation ratio of MO was only $29.10 \pm 2.33\%$ when the reaction temperature was 130 °C, the increase of reaction temperature was beneficial to improve the photocatalytic performance of the TiO_2 nanotube network. The crystalline phase content of TiO_2 was low when the reaction temperature was 130 °C, which is not conducive to the MO photocatalytic degradation. As the reaction temperature increases, TiO_2 nanotubes become longer and denser and were highly crossed on the Ti foli surface to form a network structure, which leads to a high specific surface promoting adsorption capacity. When the temperature was 160 °C, the nanotubes network structure was formed and provided a larger surface area and more reactive sites; the specific surface area of the sample was 130 m^2/g. The specific surface areas were 94 m^2/g and 111 m^2/g when hydrothermal temperature were 140 °C and 150 °C (Figure 10), respectively. Also, the specific surface area of the sample was significantly higher than the specific surface area of P25 was 50 m^2/g [30], and thus MO can be effectively degraded with the degradation ratio of about $80.00 \pm 2.33\%$. When the temperature increased to 170 °C, the TiO_2 particles on the Ti foil surface fully reacted and the dense nanotubes network structure blocks the internal space. At that time, the reactants cannot utilize the internal TiO_2 particles and then the degradation ratio of MO was $68.20 \pm 2.33\%$. Therefore, the TiO_2 nanotubes network prepared at 160 °C has the best photocatalytic performance. Meanwhile, the TiO_2 nanotubes network was compared with TiO_2 photocatalyst (P25). It was found that the photocatalytic degradation ratio of the TiO_2 nanotubes network for MO was better than that of P25 (Figure 9c).
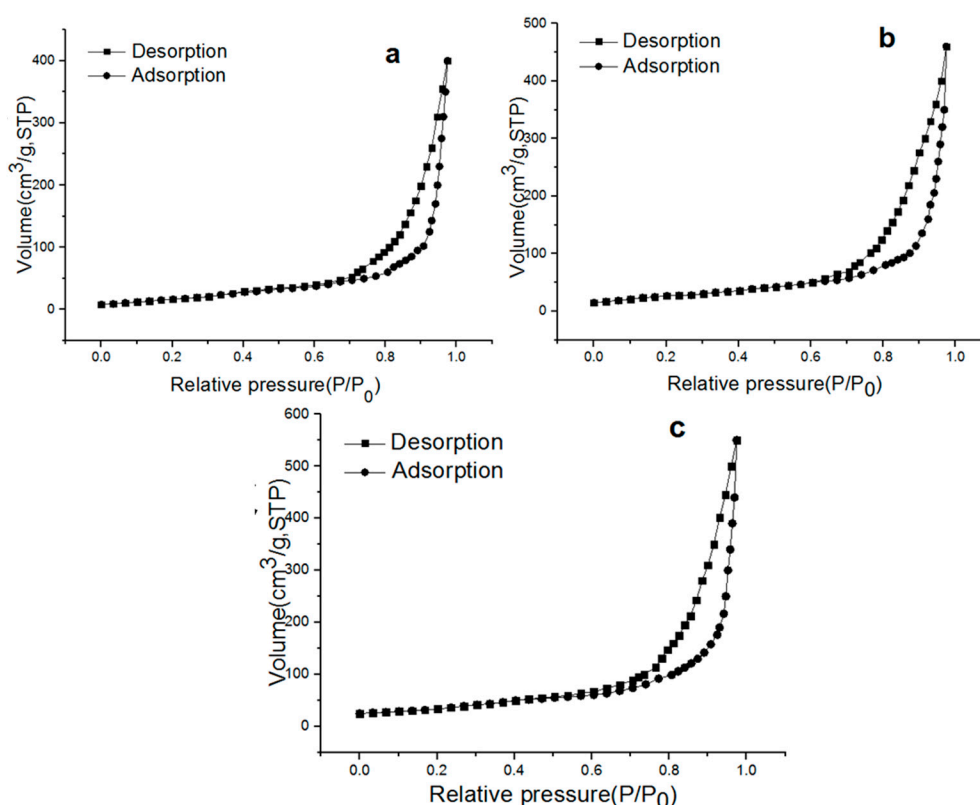

Figure 10. N_2 adsorption-desorption curves with different temperature. (**a**) 140 °C; (**b**) 150 °C; (**c**) 160 °C.

4. Conclusions

In summary, high-density and highly cross-coated anatase TiO_2 nanotube networks have been successfully prepared by alkaline hydrothermal. The optical contact angle of the TiO_2 nanotubes network was $5.1 \pm 2.9°$ when the concentration of NaOH was 10 mol/L and the reaction temperature was 160 °C, and the nanotube network reached an optimum with hydrophilic. The crystal phase content, crystallinity, density and morphology of the sample are the key factors affecting the

photocatalytic performance, when the concentration of NaOH was 7 mol/L and the reaction temperature was 160 °C. The photocatalytic activity of TiO_2 nanotubes network reached a maximum, the maximum degradation ratio of MO can reach $80.00 \pm 2.33\%$.

Author Contributions: Conceptualization, J.Y. and X.L.; methodology, J.D. and H.P.; software, J.Y.; validation, J.Y., J.D. and H.P.; formal analysis, X.L.; investigation, Y.L.; resources, C.J.; data curation, W.Q.; writing—original draft preparation, J.Y.; writing—review and editing, J.D. and H.P.; visualization, K.Z.; supervision, C.G.; project administration, R.L. and M.L.

Conflicts of Interest: The authors declare no conflict of interest.

References

1. Verlicchi, P.; Aukidy, M.A.; Zambello, E. Occurrence of pharmaceutical compounds in urban wastewater: Removal, mass load and environmental risk after a secondary treatment—A review. *Sci. Total Environ.* **2012**, *429*, 123–155. [CrossRef]

2. Polo, M.S.; Utrilla, G.P.; Pérez, R.O. Metronidazole photodegradation in aqueous solution by using photosensitizers and hydrogen peroxide. *Chem. Technol. Biotechnol.* **2012**, *87*, 1202–1208. [CrossRef]

3. Martínez, C.; Canle, L.M.; Fernández, M.I.; Santaballa, J.A.; Faria, J. Aqueous degradation of diclofenac by heterogeneous photocatalysis using nanostructured materials. *Appl. Catal. B-Environ.* **2011**, *107*, 110–118. [CrossRef]

4. Zhao, J.Z.; He, Y.; Zhang, L.; Lu, K. Preparation of porous TiO_2 powder with mesoporous structure by freeze-drying method. *J. Alloys Compd.* **2016**, *678*, 36–41. [CrossRef]

5. Yao, M.; Zhao, J.Z.; Lu, K. Preparation and hydrogenation of urchin-like titania using a one-step hydrothermal method. *Ceram. Int.* **2017**, *43*, 6925–6931. [CrossRef]

6. Chen, X.B.; Liu, L.; Peter, Y.Y.; Mao, S.S. Increasing solar absorption for photocatalysis with black hydrogenated titanium dioxide nanocrystals. *Science* **2011**, *331*, 746–750. [CrossRef]

7. Brigham, E.C.; Meyer, G.J. Ostwald isolation to determine the reaction order for $TiO_2(e-)|S^+ \rightarrow TiO_2|S$ charge recombination at sensitized TiO_2 interfaces. *Phys. Chem. C* **2017**, *118*, 7886–7893. [CrossRef]

8. Meng, J.X.; Zhang, P.C.; Zhang, F.L.; Liu, H.L.; Fan, J.B.; Liu, X.L.; Yang, G.; Jiang, L.; Wang, S.T. A self-cleaning TiO_2 nanosisal-like coating toward disposing nanobiochips of cancer detection. *ACS Nano* **2015**, *9*, 9284–9291. [CrossRef]

9. Chong, R.F.; Li, J.; Ma, Y.; Zhang, B.; Han, H.X.; Li, C. Selective conversion of aqueous glucose to value-added sugar aldose on TiO_2-based photocatalysts. *J. Catal.* **2014**, *314*, 101–108. [CrossRef]

10. Aubrey, G.D.; Chen, W.T.; Andrew, C.; Sun-Waterhouse, D.X.; Geoffrey, I.N.W. Novel Au/TiO_2 photocatalysts for hydrogen production in alcohol–water mixtures based on hydrogen titanate nanotube precursors. *J. Catal.* **2015**, *330*, 238–254.

11. Ganesh, K.M.; Mui, H.N.; Abdulhakim, A.; Khalil, A.K.; Hany, S.A.; Manoj, G. Effects of TiO_2 powder morphology on the mechanical response of pure magnesium: 1D nanofibers versus 0D nanoparticulates. *J. Alloys Compd.* **2016**, *664*, 45–48.

12. Yang, Y.; Ling, Y.C.; Wang, G.M.; Liu, T.Y.; Wang, F.X.; Zhai, T.; Tong, Y.X.; Li, Y. Photohole induced corrosion of titanium dioxide: Mechanism and solutions. *Nano Lett.* **2015**, *15*, 7051–7057. [CrossRef]

13. Chen, W.T.; Chan, A.; Zakiya, H.N.; Aubrey, G.D.; Muhammad, A.N.; SunWaterhouse, D.X.; Hicham, I.; Geoffrey, I.N.W. Effect of TiO_2 polymorph and alcohol sacrificial agent on the activity of Au/TiO_2 photocatalysts for H_2 production in alcohol–water mixtures. *J. Catal.* **2015**, *329*, 499–513. [CrossRef]

14. Jeong, N.C.; Farha, O.K.; Hupp, J.T. A convenient route to high area, nanoparticulate TiO_2 photoelectrodes suitable for high-efficiency energy conversion in dye-sensitized solar cells. *Langmuir* **2011**, *27*, 1996–1999. [CrossRef]

15. Zhou, Y.; Zhu, Q.; Tian, J.; Jiang, F. TiO_2 nanobelt@Co9S8 composites as promising anode materials for lithium and sodium ion batteries. *Nanomaterials* **2017**, *7*, 252. [CrossRef]

16. Hwang, Y.J.; Hahn, C.; Liu, B.; Yang, P. Photoelectrochemical properties of TiO_2 nanowire arrays: A study of the dependence on length and atomic layer deposition coating. *ACS Nano* **2012**, *6*, 5060–5069. [CrossRef]

17. Zhang, H.; Liu, X.; Li, Y.; Sun, Q.; Wang, Y.; Wood, B.J.; Liu, P.; Yang, D.; Zhao, H. Vertically aligned nanorod-like rutile TiO_2 single crystal nanowire bundles with superior electron transport and photoelectrocatalytic properties. *J. Mater. Chem.* **2012**, *22*, 2465–2472. [CrossRef]

18. Mancic, L.; Osman, R.F.M.; Costa, A.M.L.M.; d'Almeida, J.R.M.; Marinkovic, B.A.; Rizzo, F.C. Thermal and mechanical properties of polyamide 11 based composites reinforced with surface modified titanate nonutubes. *Mater. Des.* **2015**, *83*, 459–467. [CrossRef]

19. Kusior, A.; Kollbek, K.; Kowalski, K.; Borysiewicz, M.; Wojciechowski, T.; Adamczyk, A.; Trenczek-Zajac, A.; Radecka, M.; Zakrzewska, K. Sn and Cu oxide nanoparticles deposited on TiO_2 nanoflower 3D substrates by inert gas condensation technique. *Appl. Surf. Sci.* **2016**, *380*, 193–202. [CrossRef]

20. Sreekantan, S.; Wei, L.C. Study on the formation and photocatalytic activity of titanate nanotubes synthesized via hydrothermal method. *J. Alloy Compd.* **2010**, *490*, 436–442. [CrossRef]

21. Sun, Y.Y.; Zong, Z.M.; Li, Z.K.; Wei, X.Y. Hydrothermal synthesis of TiO_2 nanotubes from one-dimensional TiO_2 nanowires on flexible non-metallic substrate. *Ceram. Int.* **2018**, *44*, 3501–3504. [CrossRef]

22. Attar, A.S.; Mirdamadi, S.H.; Hajiesmaeilbaigi, F.; Ghamsari, M.S. Growth of TiO_2 nanorods by sol-gel template process. *J. Mater. Sci. Technol.* **2007**, *23*, 611–613.

23. Dong, S.; Wang, H.; Gu, L.; Zhou, X.; Liu, Z.; Han, P.; Wang, Y.; Chen, X.; Cui, G.; Chen, L. Rutile TiO_2 nanorod arrays directly grown on Ti foil substrates towards lithium-ion micro-batteries. *Thin Solid Films* **2011**, *519*, 5978–5982. [CrossRef]

24. Qin, L.J.; Chen, Q.J.; Lan, R.J.; Jiang, R.Q.; Quan, X.; Xu, B. Effect of Anodization Parameters on Morphology and Photocatalysis Properties of TiO_2 Nanotube Arrays. *J. Mater. Sci. Technol.* **2015**, *31*, 1059–1064. [CrossRef]

25. Liu, Z.H.; Su, X.J.; Hou, G.H.; Xiao, Z.; Jia, H.P. Hierarchical TiO_2 nanorod array for dye-sensitized solar cells. *Mater. Lett.* **2012**, *89*, 309–311. [CrossRef]

26. Li, M.; Zhang, X.M.; Liu, Y.; Yang, Y. Pr^{3+} doped biphasic TiO_2 (rutile-brookite) nanorod arrays grown on activated carbon fibers: Hydrothermal synthesis and photocatalytic properties. *Appl. Surf. Sci.* **2018**, *440*, 1172–1180. [CrossRef]

27. Barton, I.; Matejec, V.; Matousek, J. Photocatalytic activity of nanostructured TiO_2 coating on glass slides and optical fibers for methylene blue or methyl orange decomposition under different light excitation. *J. Photochem. Photobiol. A* **2016**, *317*, 72–80. [CrossRef]

28. Li, W.; Shah, S.I.; Huang, C.P.; Jung, O.; Ni, C. Metallorganic chemical vapor deposition and characterization of TiO_2 nanoparticles. *Mater. Sci. Eng. B* **2002**, *96*, 247–257. [CrossRef]

29. Du, J.; Qi, W.Q.; Zuo, J.J.; Li, X.Y.; Gu, X.; Li, K.; Zhang, K.; Gong, C.; Zou, J.G. Hydrophilic TiO_2 nanowires prepared on Ti5Si3 layer by chemical vapor deposition. *J. Chem. Res.* **2017**, *5*, 304–308. [CrossRef]

30. Natarajan, T.S.; Lee, J.Y.; Bajaj, H.C.; Jo, W.K.; Tayade, R.J. Synthesis of multiwall carbon nanotubes/TiO_2 nanotube composites with enhanced photocatalytic decomposition efficiency. *Catal. Today* **2017**, *282*, 13–23. [CrossRef]